Photoprotective Melanin Is Maintained within Keratinocytes in Storage Lysosomes

Matilde V. Neto[1,2,3], Michael J. Hall[1,2], João Charneca[1], Cristina Escrevente[1], Miguel C. Seabra[1] and Duarte C. Barral[1]

In the skin, melanin is synthesized by melanocytes within melanosomes and transferred to keratinocytes. After being phagocytosed by keratinocytes, melanin polarizes to supranuclear caps that protect against the genotoxic effects of UVR. We provide evidence that melanin-containing phagosomes undergo a canonical maturation process, with the sequential acquisition of early and late endosomal markers. Subsequently, these phagosomes fuse with active lysosomes, leading to the formation of a melanin-containing phagolysosome that we named melanokerasome. Melanokerasomes achieve juxtanuclear positioning through lysosomal trafficking regulators Rab7 and RILP. Mature melanokerasomes exhibit lysosomal markers, elude connections with the endo/phagocytic pathway, are weakly degradative, retain undigested cargo, and are likely tethered to the nuclear membrane. We propose that they represent a lysosomal-derived storage compartment that has exited the lysosome cycle, akin to the formation of lipofuscin in aged cells and dysfunctional lysosomes in lysosomal storage and age-related diseases. This storage lysosome allows melanin to persist for long periods, where it can exert its photoprotective effect efficiently.

Keywords: Keratinocyte, Lysosome, Melanin, Melanocore, Melanokerasome

Journal of Investigative Dermatology (2025) **145,** 1155–1165; doi:10.1016/j.jid.2024.08.023

INTRODUCTION

Skin pigmentation is a function of epidermal–melanin units, which are composed of approximately 1 melanocyte per 30–40 keratinocytes (KCs) (Cichorek et al, 2013). Melanocytes are the producers of the photopigment melanin. Melanin is synthesized and packaged into lysosome-related organelles termed melanosomes, but it exerts the bulk of its photoprotective effect in KCs. Therefore, melanin produced in melanocytes must be transferred to KCs and efficiently processed there. Although several transfer mechanisms have been proposed in the literature, there is now solid evidence that coupled exocytosis/phagocytosis of the melanosome core (ie, melanocore) is the predominant mode of melanin transfer in basal conditions in the human skin epidermis (Tarafder et al, 2014). In this process, melanosomes fuse with the melanocyte plasma membrane in a Rab11b- and exocyst-dependent manner, and membraneless melanocores are subsequently phagocytosed in a RAC1- and CDC42-dependent manner (Moreiras et al, 2020; Tarafder et al, 2014). After phagocytosis of melanocores by KCs (Moreiras et al, 2022), melanin-containing compartments are trafficked to the juxtanuclear region and form supranuclear caps that function akin to a parasol, protecting the nuclear DNA from harmful UVR. There are variations in the phagocytic process depending on skin color. In dark skins, large individual melanin granules are found within KCs. In contrast, in light skins, smaller granules of melanin organized in clusters are present in KCs, suggesting that the skin phototype is influenced by the differential processing of melanin (Minwalla et al, 2001).

Despite the clear importance of melanin processing in determining and maintaining skin pigmentation, the cell biology and mechanisms underlying this process remain enigmatic. Recently, we demonstrated that melanocore internalization by KCs occurs by phagocytosis, leading to the formation of a melanin-containing storage compartment, which we proposed to be named melanokerasome (MKS) (Bento-Lopes et al, 2023; Moreiras et al, 2021). MKSs were found by us and others to be weakly acidic and weakly degradative (Correia et al, 2018; Hurbain et al, 2018). We therefore proposed that they could represent either a hybrid compartment or transitional early-to-late endosomal organelles, whose maturation along the endo-lysosomal pathway had been arrested (ie, evading lysosomal fusion) (Correia et al, 2018). With recent advances in the field, it is now appreciated that lysosomes can cycle through different stages in regard to pH and acid hydrolase activity and thus can exist in a weakly acidic and poorly degradative state (Barral et al, 2022; Bright et al, 2016). Hence, we postulated that MKSs are a lysosomal compartment with special characteristics that are both unique and vital to skin pigmentation.

In this study, we characterized the melanin-containing compartment in KCs using an experimentally tractable *in vitro* model. Our data suggest that MKSs are neither hybrid

[1]*iNOVA4Health, NOVA Medical School, Faculdade de Ciências Médicas, NMS, FCM, Universidade NOVA de Lisboa, Lisboa, Portugal*

[2]*These authors contributed equally to this work.*

[3]*Current address: UCL Institute of Ophthalmology, University College London, London EC1V 9EL, UK*

Correspondence: Duarte C. Barral, NOVA Medical School, Faculdade de Ciências Médicas, Universidade NOVA de Lisboa, Campo dos Mártires da Pátria, 130, Lisboa 1169-056, Portugal. E-mail: duarte.barral@nms.unl.pt

Abbreviations: KC, keratinocyte; MKS, melanokerasome; MRCatB, Magic Red cathepsin B; TEM, transmission electron microscopy

Received 20 January 2024; revised 19 July 2024; accepted 12 August 2024; accepted manuscript published online 18 September 2024; corrected proof published online 29 October 2024

nor maturation-arrested compartments but rather mature by acquiring late endolysosomal markers and fusing with active lysosomes. Furthermore, our data suggest that MKSs utilize the lysosomal-trafficking machinery for perinuclear positioning to assist the formation of supranuclear caps. Thus, we uncovered a physiological example of lysosomes used as a storage compartment.

RESULTS

Melanin-containing compartments associate with early and late endosomes/lysosomes

Initial characterization of MKSs was performed at a single (fixed) time point and thus does not provide information about the dynamics of the maturation process and the sequence of events. To shed light on these, we designed an assay to determine whether the early and late endosomal markers are sequentially acquired over time after internalization, which would be consistent with trafficking along the endolysosomal pathway. For this, XB2 KCs were initially incubated with melanocores on ice, to allow the close contact of melanin with the cell surface but with no/minimal internalization. Phagocytosis of melanocores was then allowed by placing the cells at 37 °C. This assay will subsequently be referred in this study as a synchronized pulse of melanocores. We selected time points of 1, 4, and 24 hours after internalization to assess the transition from early to late endocytic markers at short, medium, and long time points, respectively. After phagocytosis, we observed a small but gradual decrease (~30% at 24 hours) of the early endosomal marker EEA-1 puncta surrounding phagocytosed melanocores (Figure 1a, c, and d). However, with time, there was a gradual and significant increase of the colocalization of phagocytosed melanocores with the late endosomal and lysosomal markers, CD63 and LAMP-1 (increases of up to 26 and 38%, respectively) (Figure 1b–d). Indeed, a clear transition was observed toward colocalization of late endocytic markers at later time points (Figure 1c). These observations are consistent with the hypothesis that melanin-containing phagosomes undergo maturation along the endolysosomal pathway inside KCs.

Melanin-containing phagosomes fuse with pre-existing lysosomes

We previously proposed to name the mature melanin-containing compartment in KCs MKS (Bento-Lopes et al, 2023; Moreiras et al, 2021). After establishing that this compartment is positive for late endosomal and lysosomal markers using relatively long chase periods (up to 24 hours), we next aimed to address whether MKSs are formed by fusion with a pre-existing lysosomal compartment. Using transmission electron microscopy (TEM), we first incubated XB2 KCs with a BSA-gold conjugate to load the lysosomal compartment, before feeding with melanocores for 2 hours. Within the 2-hour pulse, organelles with the lamellar morphology typically associated with lysosomes that also contained aggregated gold could be observed fusing with melanin-containing vesicles (Figure 2a). We then moved to reconstructed human pigmented epidermis as an *in vitro* human model system, which we previously showed to mimic the essential features of human pigmentation (Hall et al, 2022). We observed by TEM similar examples of melanin within compartments with lysosomal morphology (Figure 2b). We further analyzed the MKS compartment in KCs within reconstructed human pigmented epidermis by serial section transmission electron tomography (volume TEM) to more closely visualize MKS content. We identified melanin within juxtanuclear single-membraned MKSs, also containing other membranes that likely represent lysosomal cargo such as intralumenal vesicles and lysosomal lamellae (Figure 2c). Tomography also revealed a striking close apposition between the outer nuclear envelope membrane and the MKS-limiting membrane, which could be maintained by tethers (Supplementary Figure S1).

It was previously reported that the recruitment of RILP by Rab7 and its consequent binding to the dynein–dynactin motor complex promote the emission of tubular protrusions that allow the fusion of late phagosomes and lysosomes (Harrison et al, 2003). This led us to inquire whether Rab7 could also mediate the fusion between melanin-containing phagosomes and lysosomes. To address this question, we performed a pulse-chase assay to load lysosomes with fluorescent dextran. KCs were then simultaneously incubated with melanocores and treated with the Rab7 competitive inhibitor CID1067700 (Agola et al, 2012) or vehicle, and the colocalization between dextran and melanocores was assessed by live imaging. The results showed a significant decrease (~41%) in the colocalization between melanocores and dextran in cells treated with the Rab7 inhibitor, indicating that Rab7 regulates the fusion between melanin-containing phagosomes and lysosomes (Figure 2d). Overall, these results suggest that after internalization by KCs, melanin-containing phagosomes undergo maturation along the endocytic pathway, which culminates in their fusion with lysosomes, originating a specialized lysosomal compartment—the MKS.

MKS juxtanuclear positioning is dependent on Rab7 and RILP

In KCs, melanin accumulates in the juxtanuclear region. Because MKSs are specialized phagolysosomes, we hypothesized that the molecular machinery involved in the transport of MKSs to the juxtanuclear region of KCs is shared with lysosomes. Lysosome positioning depends on their long-range transport along microtubules, which is regulated by the relative activity of the motor proteins dynein and kinesins (Harada et al, 1998; Hollenbeck and Swanson, 1990; Matteoni and Kreis, 1987; Pu et al, 2016). The anterograde transport of lysosomes is predominantly regulated by the interaction between Arl8b and the BLOC1-related complex (Pu et al, 2015). Arl8b- BLOC1-related complex can mediate the direct binding of lysosomes to kinesin-3 or the indirect binding of lysosomes to kinesin-1, through the recruitment of the Arl8b effector PLEKHM2 (also known as SKIP) (Guardia et al, 2016; Khatter et al, 2015; Rosa-Ferreira and Munro, 2011). Accordingly, we observed that the overexpression of Arl8b promotes an accumulation of both LAMP-1-positive vesicles and MKSs at the periphery of KCs, which suggests that the transport of MKSs in KCs is regulated by the same molecular mechanisms as lysosomal positioning (Supplementary Figure S2).

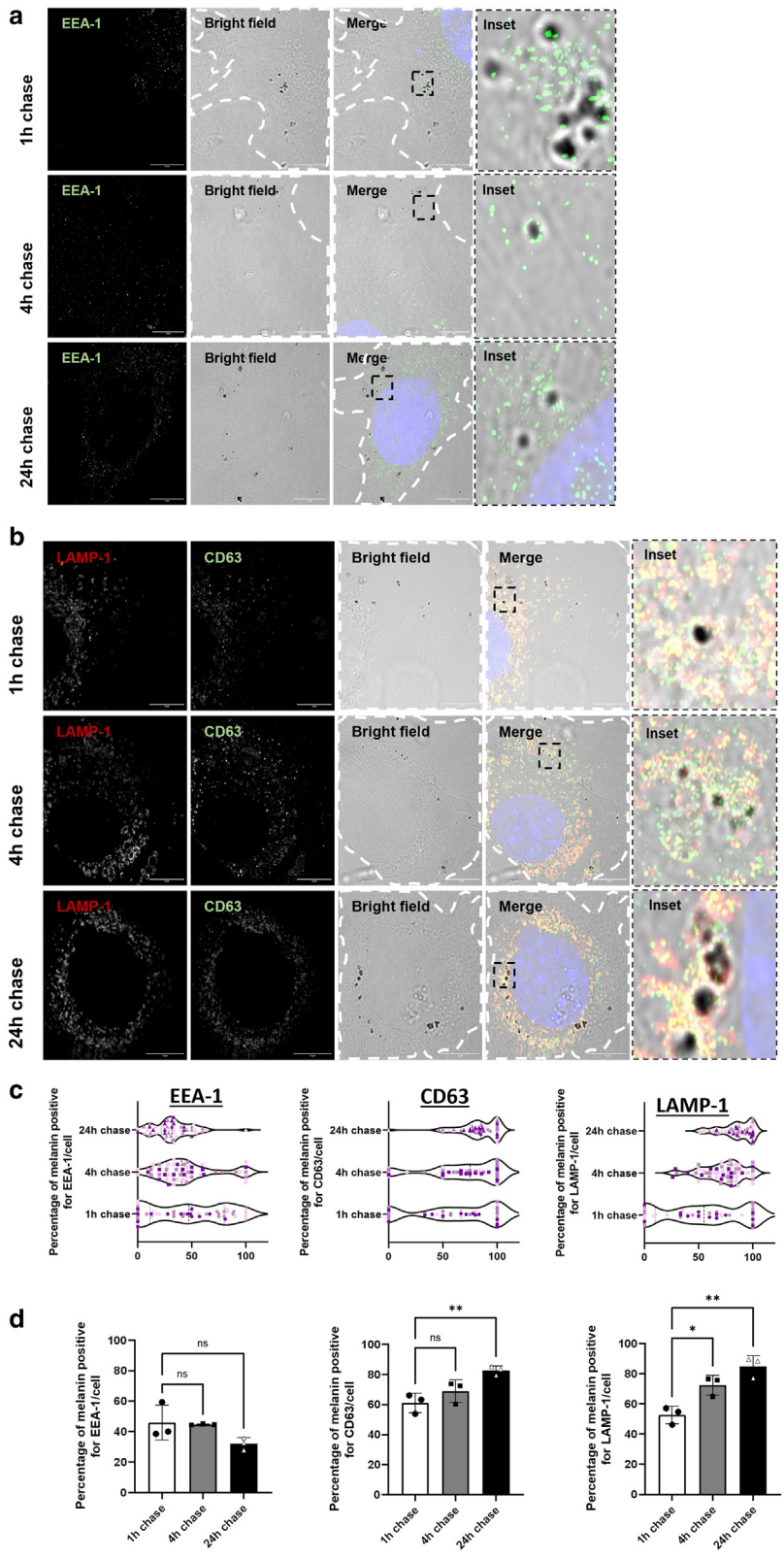

Figure 1. Association of melanin-containing compartments with LAMP-1 and CD63 increases over time after phagocytosis. XB2 keratinocytes were incubated with melanocores for 1 hour and washed, and melanin was chased for 1, 4, or 24 hours. After the chase, cells were fixed, and early endosomes were identified by the presence of **(a)** EEA-1 and **(b)** late endosomes/lysosomes by CD63 and LAMP-1 labeling using immunofluorescence. Nuclei were visualized by DAPI staining (blue). Bars = 10 μm. **(c, d)** Violin plots and bar plots representing the quantified percentage overlap of EEA-1, CD63, and LAMP-1 with melanin detected by brightfield at the different chase time points are shown, respectively. *P* values (One-way ANOVA) were considered statistically significant (*) and (**) when <.01 and <.05, respectively, or ns when ≥.05. Plots show mean ± SD of 3 independent experiments. ns, nonsignificant.

On the other hand, the retrograde transport of lysosomes is mainly mediated by Rab7. After activation, Rab7 recruits its effector RILP, which binds to the light intermediate chain of dynein and to the p150^{Glued} subunit of dynactin, promoting the transport of lysosomes toward the juxtanuclear region of the cells (Cantalupo et al, 2001; Jordens et al, 2001). To assess whether Rab7 regulates the transport of MKSs in KCs, we silenced either Rab7a and/or Rab7b and observed an

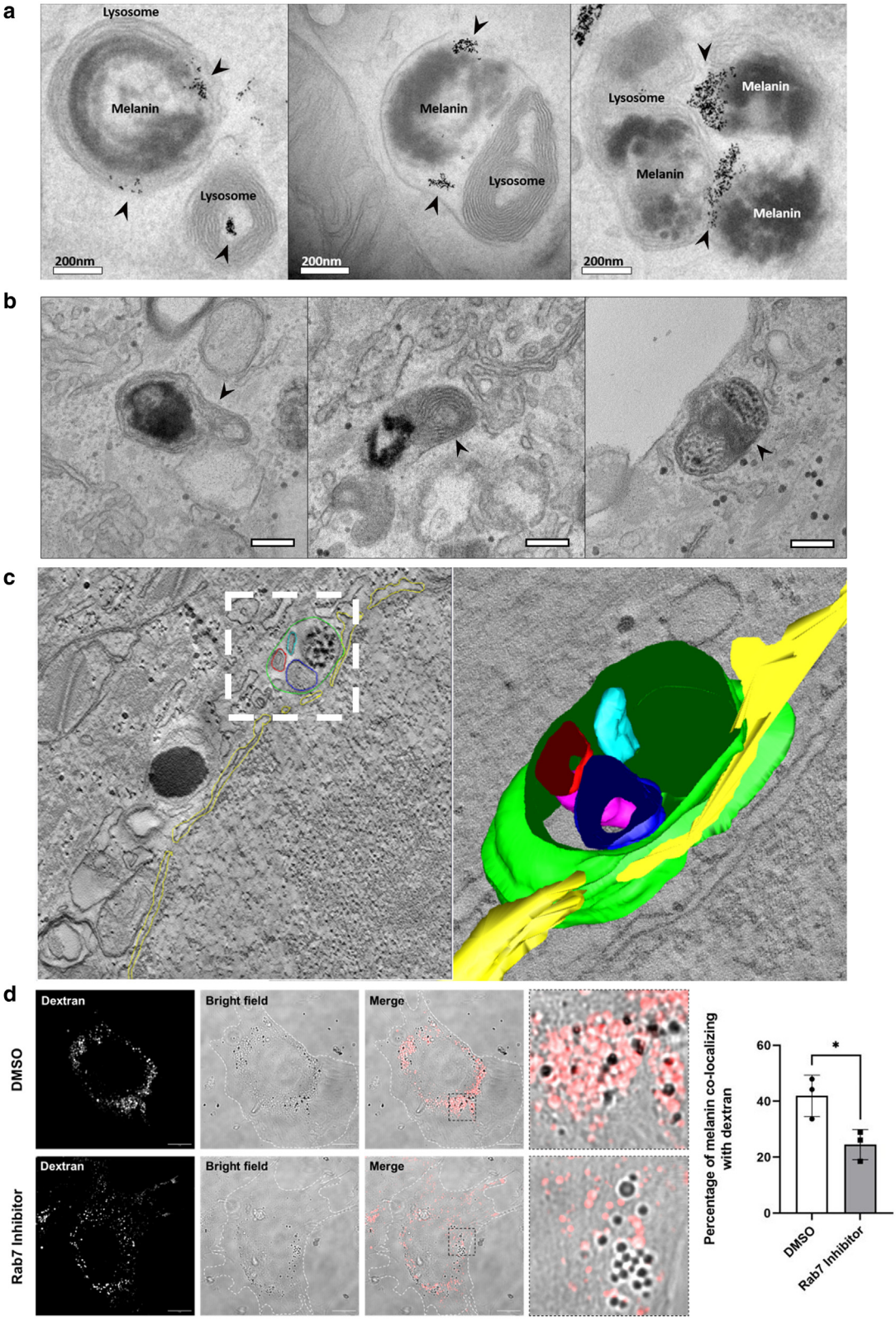

Figure 2. Melanin-containing phagosomes fuse with lysosomes, and the resulting MKSs exhibit lysosome-like morphology. **(a)** XB2 keratinocytes were pulsed with BSA-gold conjugate (5 nm Au, arrows) for 2 hours and chased for 1 hour to load the lysosomal compartment and then pulsed with melanocores for 2 hours and fixed immediately after the pulse. Melanin-containing phagosomes can be observed fusing with gold-containing lysosomes when observed by TEM. Bars = 200 nm. **(b)** Examples of MKSs with lysosome-like morphology (arrows) are shown in reconstructed human pigmented epidermis keratinocytes. Bars = 200 nm. **(c)** An MKS positioned close to the nuclear envelope (yellow) was imaged 3-dimensionally by transmission electron tomography, revealing the presence of lysosomal lamellae (blue) and intralumenal vesicles (red, turquoise) enclosed within the same single membraned compartment (green) as the melanin. **(d)** XB2 keratinocytes were incubated with fluorescent dextran to load lysosomes before incubating with a Rab7 inhibitor (CID1067700) and then feeding with melanocores. Colocalization between dextran and melanin was quantified. Bars = 10 μm. Quantification represents a minimum of 50 cells per condition. MKS, melanokerasome; TEM, transmission electron microscopy.

impairment in the juxtanuclear clustering of MKSs in the cells silenced for Rab7a/b, compared with that in control cells (Figure 3a and c). In addition, we found that the silencing of Rab7a/b promotes a dispersion of LAMP-1-positive vesicles. These phenotypes were also observed when we used the Rab7 inhibitor CID1067700 (Supplementary Figure S2). Because RILP promotes the interaction between Rab7 and the dynein/dynactin motor complex (Cantalupo et al, 2001; Jordens et al, 2001), we next assessed whether RILP is involved in the transport of MKSs to the juxtanuclear region of KCs. As expected, we observed a dispersion of MKSs as well as LAMP-1-positive vesicles in cells depleted of RILP (Figure 3b and d). These results suggest that Rab7 and its effector RILP mediate the retrograde transport of MKSs to the juxtanuclear region of KCs.

Melanin persists in a storage lysosome

Previous work from our group established that melanin persists in KCs for at least 7 days (Correia et al, 2018). Therefore, we aimed to understand how melanin is able to evade degradation, despite fusion of melanin-containing phagosomes with lysosomes. Although previous studies appeared to point toward the arrested maturation hypothesis (Correia et al, 2018; Hurbain et al, 2018), a more recent unveiling of the lysosome complex dynamics (Barral et al, 2022; Bright et al, 2016, 1997) raised the possibility that MKSs exist in a hydrolase-inactive stage of the lysosome cycle after acquisition of melanin. Therefore, we measured lysosomal hydrolase activity by flow cytometry at different time points after melanocore internalization using Magic Red cathepsin B (MRCatB). MRCatB is membrane-permeable probe that fluoresces upon cleavage by cathepsin B and thus can be utilized as a specific readout of lysosome activity. We observed no significant differences in MRCatB fluorescence at 1 and 4 hours, compared with the observation in control cells that were not fed melanin (Figure 4a and b). Conversely, 24 hours after melanin internalization, we observed a significant decrease in the fluorescence of MRCatB, which suggests a reduction in lysosomal hydrolase activity caused by the presence of melanin inside lysosomes.

It has been suggested that lysosomes in certain stages of the lysosome cycle or dysfunctional lysosomes can be less fusogenic and thus less accessible to newly internalized material (Cardoso et al, 2023; Escrevente et al, 2021). Therefore, we analyzed whether preformed MKSs are accessible to newly internalized fluid-phase cargo. To do so, XB2 cells were fed with melanocores, chased for either 4, 24, or 72 hours, and then pulse-chased with fluorescent dextran. We observed no significant differences in MKS accessibility to dextran between 4 and 24 hours (Figure 4c and d). At 72 hours, we were able to detect a reduction in fluorescent puncta colocalizing with MKSs, which indicates that these mature compartments lose their ability to fuse with late endosomes/lysosomes (Figure 4d). Altogether, the observed decreases in lysosomal hydrolase activity and accessibility to the endolysosomal pathway at later time points suggest that these compartments drop out of the lysosome cycle as they mature, and therefore represent lysosomes in the terminal stage of their life cycle.

DISCUSSION

In this study, we unravel the cellular mechanisms underlying melanin processing and fate after transfer to KCs to achieve efficient photoprotection. The results presented suggest that melanin-containing phagosomes mature along the endolysosomal pathway and fuse with lysosomes and that melanin resides within a terminal lysosomal compartment, likely tethered to the nuclear membrane and inaccessible by the endolysosomal pathway (Figure 5).

We observed a time-dependent and significant increase in the number of melanin-containing phagosomes associating with the late endosomal/lysosomal markers CD63 and LAMP-1 after melanocore internalization, in addition to presenting evidence that these compartments fuse with pre-existing lysosomes. This suggests that after phagocytosis by KCs, melanin-containing phagosomes undergo maturation along the canonical endocytic pathway, which is contrary to the alternative hypothesis that the MKS represents a maturation-arrested compartment. Notably, our results showed only a small decrease in the number of EEA1-positive vesicles surrounding melanin-containing phagosomes with time. Importantly, recent studies found that EEA-1 only partially colocalizes with Rab5-positive vesicles and is also recruited to late endosomes (van der Beek et al, 2022), suggesting a more widespread distribution of this marker than previously accepted. Because MKSs originate from the fusion between melanin-containing phagosomes and lysosomes, this led us to hypothesize that transport of the former to the juxtanuclear region of KCs relies on similar mechanisms and machinery that regulate lysosome positioning. In fact, we observed that the overexpression of Arl8b induces the dispersion of melanin throughout the cytoplasm of KCs, which is in agreement with this protein regulating the kinesin-dependent trafficking of lysosomes toward the periphery of the cells (Niwa et al, 2016; Rosa-Ferreira and Munro, 2011).

We also hypothesized that MKSs utilize lysosomal-trafficking machinery as an efficient redundancy mechanism to form the terminal compartment and establish juxtanuclear positioning, which could play a role in the formation of supranuclear caps. Indeed, we found that the silencing of Rab7 or RILP significantly impairs the retrograde transport of MKSs inside KCs. Strikingly, this phenotype was observed not only with the silencing of Rab7a but also Rab7b. Whereas Rab7a plays a well-known role in endosome maturation and lysosomal trafficking, Rab7b was described to control the late endosome-to-*trans*-Golgi network transport (Progida et al, 2010). Nevertheless, a recent study reported that melanosomes internalized by KCs are stored in compartments that are positive for Rab7b (Marubashi and Fukuda, 2020).

We also provide evidence that melanin-loaded lysosomes of KCs have reduced lysosomal hydrolase activity after prolonged chase periods and that MKSs become less accessible to newly endocytosed fluid phase cargo. Considering that melanin is known to be a dense polymer that is resistant to degradation by biochemical means (Borovanský and Elleder, 2003) and because, to our knowledge, no concrete evidence demonstrating melanin degradation in mammalian cells has been put forward, we

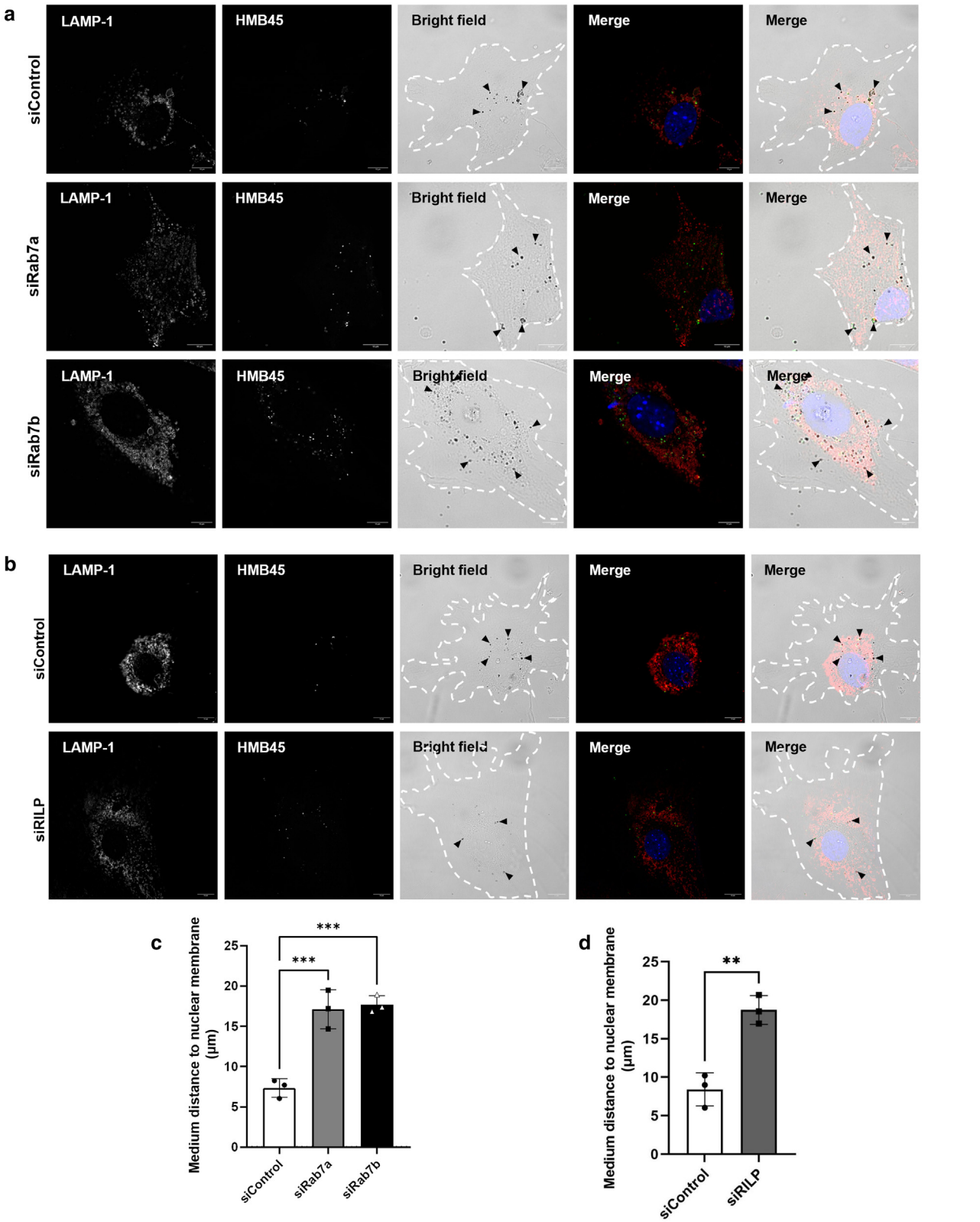

Figure 3. Impaired MKS juxtanuclear positioning upon modulation of lysosomal positioning machinery components. **(a, b)** XB2 keratinocytes were transfected with nontargeting siRNA (siControl), siRab7a, **(a)** siRab7b, or **(b)** siRILP. Cells were then incubated with 0.1 g/l of melanocores for 4 hours, and melanin was chased for another 20 hours. After the chase, cells were fixed, and the distribution of melanocores inside keratinocytes was assessed by immunofluorescence, with the LAMP-1 (red) and HMB45 (green) antibodies. Nuclei were visualized by DAPI staining (blue). Bars = 10 µm. Arrowheads indicate the melanocores inside keratinocytes. Quantification of the mean distance of melanocores to the nuclear envelope after the silencing of **(c)** Rab7a and Rab7b or **(d)** RILP. *P*-values (One-way ANOVA) were considered statistically significant when <.001 (***) or when <.01 (**). Plots show mean ± SD of 3 independent experiments. MKS, melanokerasome; siControl, nontargeting small interfering RNA; siRab7a, Rab7a-targeted small interfering RNA; siRab7b, Rab7b-targeted small interfering RNA; siRILP, RILP-targeted small interfering RNA; siRNA, small interfering RNA.

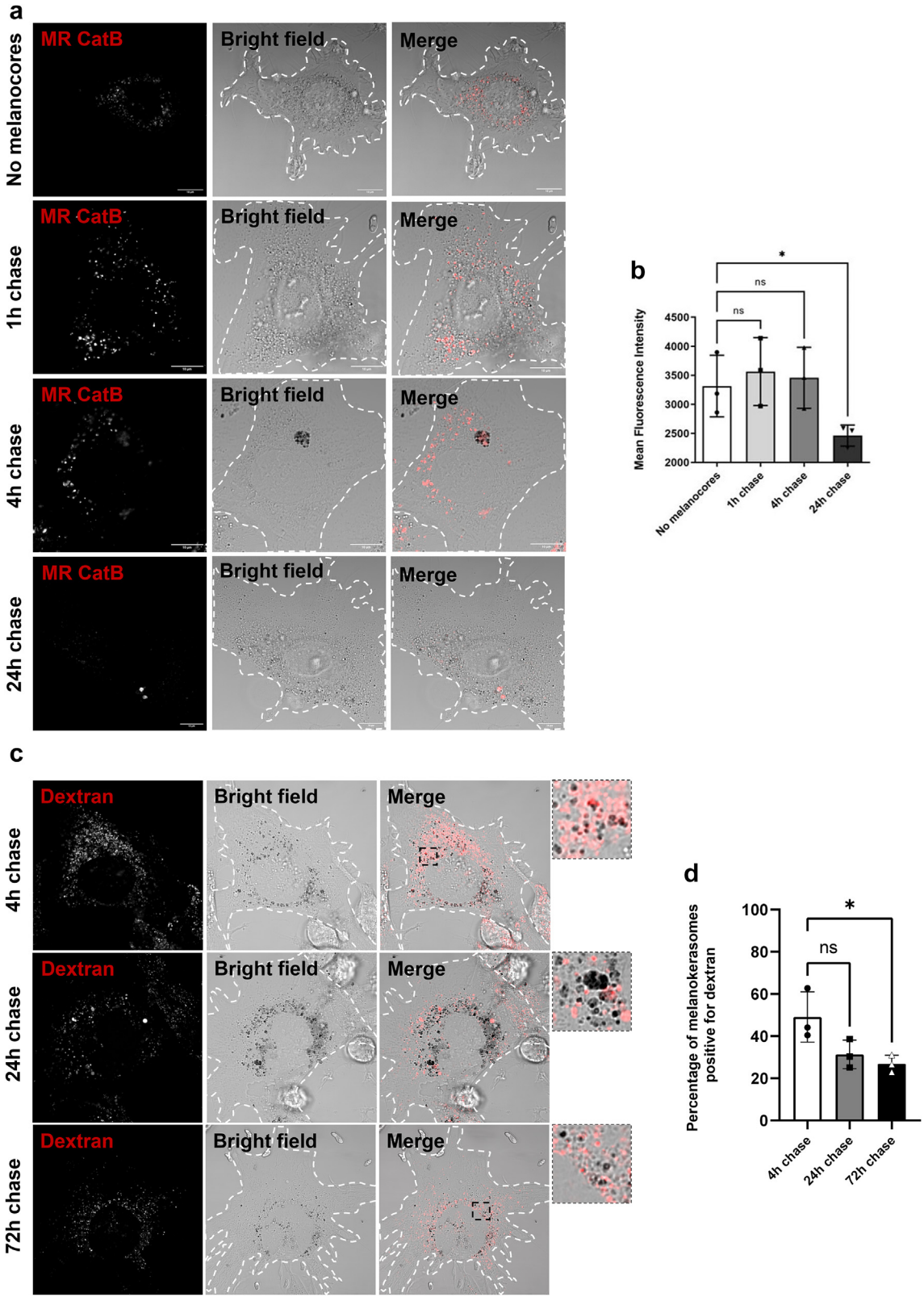

Figure 4. MKS maturation is accompanied by a reduction in lysosomal hydrolase activity and decreased accessibility to fluid phase cargo. (a, b) XB2 keratinocytes were fed with melanocores and chased for varying periods of time (1, 4, or 24 hours), and CatB activity was assessed using MRCatB. Representative confocal images of MRCatB fluorescence are shown in **a**, and quantitative analysis of CatB activity performed by flow cytometry is shown in **b**. Bars = 10 μm. *P*-values (One-way ANOVA) were considered statistically significant when <.05 (*) or ns when ≥.05. Plots show mean ± SD of 3 independent experiments. **(c, d)** XB2 keratinocytes were fed with melanocores and chased for varying periods of time (4, 24, or 72 hours) and then pulsed and chased with dextran Alexa Fluor 568 to load the terminal endolysosomal compartment. The percentage of MKSs accessible to the newly endocytosed dextran was measured through the colocalization between melanin (brightfield) and dextran. Bars = 10 μm. *P*-values (One-way ANOVA) were considered statistically significant when <.05 or ns when ≥.05. Plots show mean ± SD of 3 independent experiments. CatB, cathepsin B; MKS, melanokerasome; MRCatB, Magic Red cathepsin B; ns, nonsignificant.

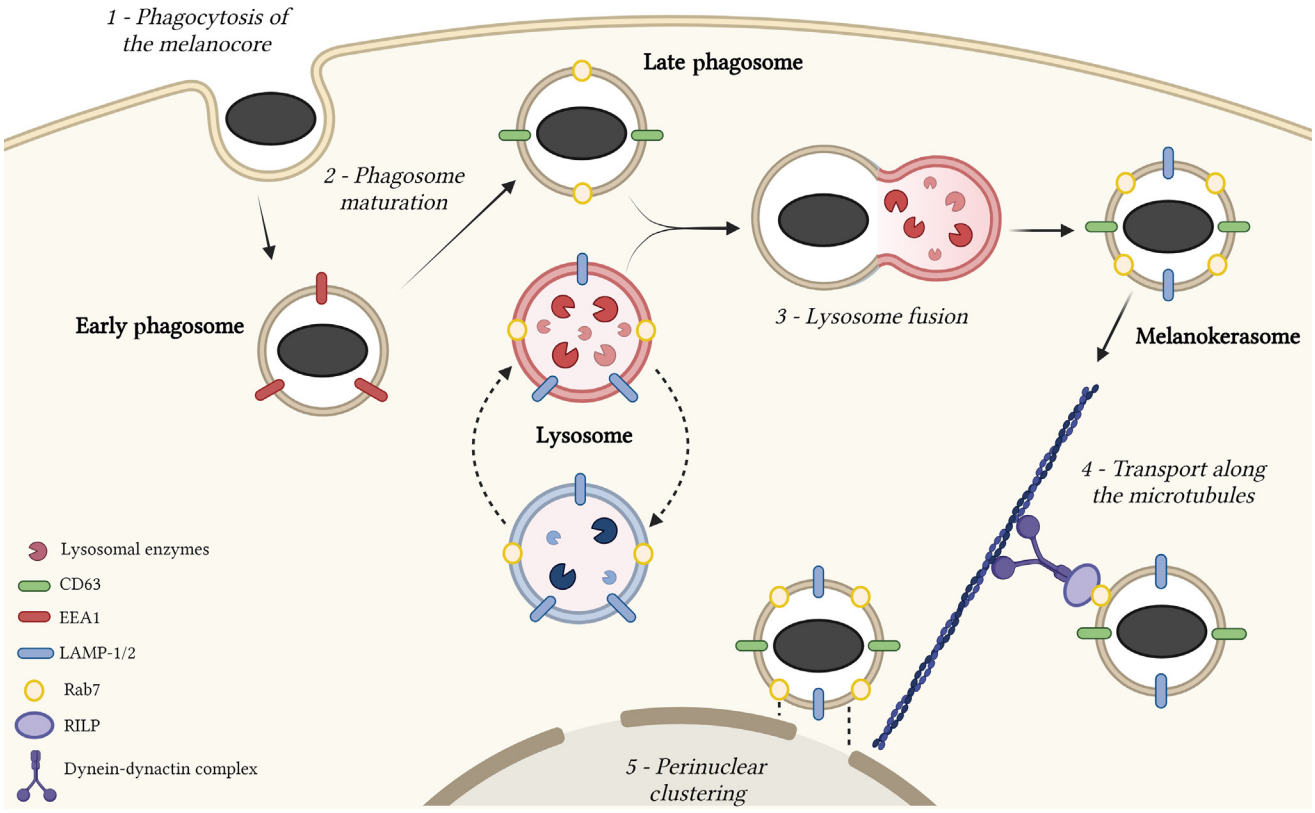

Figure 5. Schematic representation of the working model of MKS formation and maturation. (1) Melanocores secreted by melanocytes are phagocytosed by keratinocytes and **(2)** sequentially acquire early and late endolysosomal markers before fusion with lysosomes to form MKSs **(3)**. **(4)** These are transported toward the nucleus using canonical lysosomal positioning machinery and **(5)** cluster around the apical pole of the nucleus to form photoprotective parasol-like supranuclear caps. MKS, melanokerasome. Created in BioRender. Seabra, MC (2024) BioRender.com/g93r788.

propose that MKSs represent a storage lysosome. Indeed, it would be energetically favorable for cells to maintain MKSs in this state and ensure that melanin persists for long periods without significant degradation.

The characteristics of the MKS we found, namely, exhibiting lysosomal markers, eluding connections with the endo/phagocytic pathway, being weakly acidic/degradative, and retaining undigested cargo (melanin), have been ascribed to dysfunctional lysosomes in pathological processes, from hereditary lysosomal storage diseases to neurodegenerative diseases (Burrinha et al, 2023; Nixon, 2020). This is also the case in the formation of lipofuscin-like autofluorescent granules in retinal pigment epithelial cells implicated in age-related macular degeneration (Escrevente et al, 2021). Therefore, we suggest that undigested cargo material, the loss of hydrolytic activity, and increased pH lead MKSs to drop out of the lysosome cycle and become storage (dysfunctional) lysosomes. MKSs could thus represent the physiologically beneficial parallel to lysosome dysfunction. Understanding further the mechanisms leading to the creation of storage lysosomes may help elucidate critical pathogenic mechanisms in age-related diseases and uncover novel therapeutic approaches targeting the lysosome and endolysosomal-trafficking machinery.

In this study's context, we focused on characterizing the formation of the melanin storage compartment in KCs, a fundamental topic that has remained enigmatic. Given the appreciated influence of melanin processing by KCs in determining skin phototype in different individuals, future studies should build on the findings of this study to investigate whether differential processing of melanin by KCs could affect overall skin pigmentation, providing insights of high value for the pharmaceutical and cosmetic industries.

MATERIALS AND METHODS

Cell culture and reconstructed human pigmented epidermis

XB2 murine KCs were cultured in DMEM (Gibco/Invitrogen), supplemented with 10% fetal bovine serum, 2 mM L-glutamine, 100 U/ml penicillin, and 100 U/ml streptomycin. MNT1 human melanoma cells were cultured in DMEM, supplemented with 10% fetal bovine serum, 2 mM L-glutamine, 1% nonessential amino acids (Gibco/Invitrogen), 100 U/ml penicillin, and 100 U/ml streptomycin. Cells were maintained at 37 °C, 10% carbon dioxide, and 95% humidity. Reconstructed human pigmented epidermis was formed from commercially available primary cells purchased from CellnTec, as previously described (Hall et al, 2022; Zoio et al, 2021). Briefly, primary melanocytes and primary KCs were seeded upon a polycarbonate membrane, and KC differentiation and stratification were induced by establishing an air–liquid interface.

Isolation of melanocores

MNT1 melanoma cells were cultured for 7 days in 150 cm^2 T flasks (Corning) in complete growth medium. Afterward, the culture medium, referred to as conditioned medium in the remaining parts of this paper, was collected and concentrated by sequential

centrifugations of 30 minutes at 3800*g* in a Vivaspin Centricon (Sigma), with a pore size of 300 kDa. The absorbance value of the melanocore preparation was measured using a Nanodrop 2000 (Thermo Fisher Scientific) at 340 nm, and the concentration of melanin was calculated using a calibration curve developed in-house: (absorbance = 1.8546 × concentration [g/l] − 0.0422).

Small interfering RNA silencing

XB2 KCs were seeded in 24-well plates, at a confluency of 4×10^4 cells per well. Twenty-four hours later, 50 nM of small interfering RNA pools (Thermo Fisher Scientific) (Supplementary Table S1) were added to 50 μl of Opti-MEM (Gibco/Invitrogen). Simultaneously, 1.5 μl of Dharmafect 4 (Dharmacon) was diluted in 50 μl of Opti-MEM. Both mixtures were incubated at room temperature for 5 minutes and then combined, mixed gently, and incubated for 20 minutes at room temperature. Culture medium was removed before transfection, and 100 μl of small interfering RNA mixture was added to 400 μl of Opti-MEM. Cells were then incubated in normal culture conditions, and 24 hours later, the transfection medium was replaced with complete growth medium. A nontargeting small interfering RNA pool (Thermo Fisher Scientific) (Supplementary Table S1) was used as a control. Efficient silencing was validated by real-time quantitative reverse transcription PCR analysis (Supplementary Figure S3).

Plasmid transfection

XB2 cells were seeded in 24-well plates, at a confluency of 4×10^4 cells per well. Twenty-four hours after seeding, a mixture of 1 μg of plasmid (Supplementary Table S2) in 100 μl of Opti-MEM was combined with 1.5 μl of TurboFect (Thermo Fisher Scientific), diluted in 100 μl of Opti-MEM, according to the manufacturer's instructions. Cells were then incubated for 24 hours in normal culture conditions, and the medium was changed to 500 μl of complete growth medium. The plasmids used are presented in Supplementary Table S2.

Real-time quantitative PCR

Total RNA was isolated using the RNeasy Mini kit (Qiagen), according to the manufacturer's instructions. Superscript II DNA synthesis kit (Invitrogen) was used to reverse transcribe 500 ng to 1 μg of total RNA and synthesize cDNA. Real-time quantitative reverse transcription PCR reactions were performed using a Roche LightCycler and the Roche SybrGreen Master Mix reagent. The reaction mixture was composed of 5 μl of SybrGreen, 4 μl of cDNA, and 10 μm of specific primers (Supplementary Table S3) for a total reaction volume of 10 μl. For each protein, gene expression was calculated relative to control wells with LightCycler96 software (Roche). *GAPDH* was used as a housekeeping gene. Quadruplicates were used for each gene.

Immunofluorescence

Cells were fixed with 4% paraformaldehyde in 1X PBS for 20 minutes. The excess of fixative was removed by washing with 1X PBS for 10 minutes, and permeabilization and blocking were performed with a solution of 1% (m/v) BSA (Sigma-Aldrich) and 0.05% (m/v) saponin (Sigma-Aldrich) in 1X PBS for 30 minutes. The cells were then incubated with diluted primary antibodies (Supplementary Table S4) for 1 hour and 30 minutes, washed 3 times with 1X PBS, and subsequently incubated for 1 hour with Alexa fluorophore–conjugated secondary antibodies diluted 1:500 in blocking buffer (Supplementary Table S4). Unbound antibodies were removed with extensive washing with 1X PBS. In the specific case of the immunostaining with HMB45 and anti-LAMP-1 antibodies, the latter was added after the incubation with the secondary antibody and after extensive washing with 1X PBS to avoid any unspecific cross-reactions. Coverslips were then mounted on glass slides with the Fuoromount-G mounting media containing DAPI (Invitrogen) to stain the nuclei of the cells. All antibody incubations and washes were performed with a solution of 1% (m/v) BSA and 0.05% (m/v) saponin and 1X PBS, respectively. All steps were performed at room temperature.

Cathepsin B activity assay

Cathepsin B activity was detected and measured using MRCatB substrate from ImmunoChemistry Technologies, which fluoresces upon cleavage by active cathepsin B. Briefly, MRCatB was added to cells for 30 minutes prior to imaging/fluorescence measurement at the manufacturer's recommended dilution in normal culture conditions, and fluorescence was measured by flow cytometry. For each condition, a parallel glass coverslip of cells with identical treatment was imaged by live-cell confocal microscopy to provide representative images and to confirm probe specificity.

Flow cytometry

XB2 cells incubated with MRCatB were washed with PBS and flow cytometry buffer (1% fetal bovine serum [v/v] and 2 mM EDTA in PBS), centrifuged at 300*g* for 5 minutes, and resuspended in flow cytometry buffer. Data acquisition was performed in a FACS CANTO II flow cytometer (BD Biosiences). At least 30,000 cells were acquired per condition using BD FACSDivaTM software (version 6.1.3, BD Biosciences). Data analysis was performed in FlowJo (version 10, BD Biosciences).

Lysosome loading with dextran

XB2 KCs were plated on Nunc Lab-Teks (Thermo Fisher Scientific) at a confluency of 1.5×10^4 cells per well. The following day, 1 mg/ml of dextran Alexa Fluor 568 (10 kDa, Invitrogen) was fed to the cells for 4 hours and chased for 20 hours to accumulate in lysosomes. Then, KCs were incubated with 0.1 g/l of melanocores for 4 hours and chased for 20 hours and the colocalization between dextran and melanin was assessed by live-cell imaging. To determine whether MKSs are accessible to fluid phase cargo, XB2 cells were pulsed with melanocores for 1 hour on ice and then chased for 4, 24, or 72 hours. Although the cells were being chased, they were also pulsed with dextran for 2 hours and chased for another 2 hours. After this, live imaging of the cells was performed by confocal microscopy.

Preparation and loading of BSA-gold conjugate

After performing a stabilization test to determine the amount of protecting BSA (Sigma-Aldrich) required to stabilize a fixed volume of 5 nm gold colloid suspension (BBI Solutions), the appropriate volumes of BSA in 2 mM borax and 20 ml gold colloid suspension were combined. After gentle agitation for 5 minutes, the preparation was secondarily stabilized with a solution of 10% BSA in 2 mM borax to a final concentration of 1% BSA. The preparation was centrifuged at 205,250*g* for 25 minutes, and the fluid pellet containing the BSA-gold conjugate was extracted. The final fluid pellet formed from 22.5 ml of the starting gold colloid suspension was diluted 1:7 in media and fed to the cells, as with dextran.

Melanin distribution quantification

XB2 KCs transfected with small interfering RNAs (Supplementary Table S1) or incubated with 25 nM of a Rab7 inhibitor (CID-1067700, Sigma-Aldrich) were then fed with 0.1 g/l of melanocores for 4 hours, and melanin was chased for another 20 hours. After the chase, cells were fixed, and the distribution of late endosomes/lysosomes and melanin-containing compartments inside KCs was assessed by immunofluorescence, with anti-LAMP-1 and HMB45 antibodies (Supplementary Table S4), respectively. Brightfield microscopy was also used to identify dark melanin-containing compartments. Melanin distribution was assessed by an ImageJ macro developed and kindly shared by Silvia Benito-Martínez and Cédric Delevoye (Institut Curie). Nuclei were counted to ensure similar cell confluence in all samples.

Fluorescence microscopy

Confocal imaging was performed with a Zeiss LSM980 confocal microscope, equipped with a ×40 1.1 numerical aperture water objective and ×63 1.4 numerical aperture oil objective, and live imaging was performed at 37 °C in 4-(2-hydroxyethyl)-1-piperazineethanesulfonic acid buffer/media. Super-resolution images were acquired using the Airyscan 2 detector (Zeiss).

TEM

All reagents and materials were purchased from Electron Microscopy Sciences unless otherwise stated. Specimens were fixed in 2% paraformaldehyde and 2% glutaraldehyde in 0.1 M sodium phosphate buffer overnight at 4 °C. Specimens were postfixed for 1 hour on ice using 1% osmium tetroxide and 1.5% potassium ferrocyanide in distilled water, and then incubated with 1% tannic acid in distilled water for 30 minutes at room temperature before dehydrating with a series of increasing ethanol concentrations (70%, 90%, 2× 100%) and infiltrating/embedding in Epon resin (EMbed 812). After polymerizing resin at 65 ºC overnight, glass was removed by immersion in liquid nitrogen in the case of cell monolayers, and resin blocks were sectioned at 70 nm thickness using a Reichart Ultracut S ultramicrotome (Leica) and a diamond knife (Diatome), and sections were collected on copper mesh grids. Sections were post-stained with 2% uranyl acetate in 70% methanol followed by Reynold's lead citrate and imaged with a Hitachi H-7650 TEM equipped with an AMT XR41 M digital camera.

For tomography, 1 × 1 mm squares reconstructed human pigmented epidermis were embedded as described earlier before serial sectioning at 120 nm thickness using a Leica UC7 and placing section ribbons on formvar-coated copper slot grids. Single-axis tilt series (±60°) were acquired from 5 sequential serial sections using SerialEM software (developed at University of Colorado Boulder) with an FEI Tecnai G2 Spirit BioTWIN TEM equipped with an Olympus-SIS Veleta CCD camera. Tomogram generation was performed by back projection in IMOD (developed at University of Colorado Boulder), and segmentation and surface rendering were performed using the 3dmod interface in IMOD.

Image and statistical analysis

All optical microscopy images for this manuscript were analyzed using ImageJ software. A minimum of 3 independent experiments were performed as replicates, with at least 50 cells imaged and quantified per condition/replicate. Graphic representation and statistical analysis were performed in Prism (GraphPad Software). Student's *t*-test and One-way ANOVA were used to analyze the *P*-value of differences between 2 or more conditions, respectively.

ETHICS STATEMENT

All commercial human neonatal cells were derived from tissues obtained from accredited institutions, including tissue and organ procurement organizations, qualified research tissue organizations, and prominent academic and medical centers, through collaborations that follow rigorous regulations, certifications, and/or accreditations. Tissues obtained through these source facilities, which are under nondisclosure agreements, are consistent with the legal and ethical practices of the United States and the European Union, following the United States federal guidance on the use of human subjects in research (45 CFR part 46, subparts A, B, C, and D); the Health Insurance Portability and Accountability Act, which addresses issues of confidentiality of personal information; the National Organ Transplant Act (42 CFR part 482); and the Uniform Anatomical Gift Act of 1968, revised in 1984. Written informed consent was obtained by these institutions from the donor or the donor's legal next of kin for use of the tissue and its derivatives for research purposes. The use of these cells was approved by the NOVA Medical School, Faculdade de Ciências Médicas Ethics Committee (98/2022/CEFCM).

DATA AVAILABILITY STATEMENT

No datasets were generated or analyzed during this study.

ORCIDs

Matilde V. Neto: http://orcid.org/0000-0003-2267-6397
Michael J. Hall: http://orcid.org/0000-0002-1579-1488
João Charneca: http://orcid.org/0000-0002-3154-5711
Cristina Escrevente: http://orcid.org/0000-0002-2183-3947
Miguel C. Seabra: http://orcid.org/0000-0002-6404-4892
Duarte C. Barral: http://orcid.org/0000-0001-8867-2407

CONFLICT OF INTEREST

The authors state no conflict of interest.

ACKNOWLEDGMENTS

This work was supported by iNOVA4Health (UIDB/04462/2020 and UIDP/04462/2020) and by the Associated Laboratory LS4FUTURE (LA/P/0087/2020) two programs financially supported by Fundação para a Ciência e Tecnologia/Ministério da Ciência, Tecnologia e Ensino Superior—as well by Fundação para a Ciência e Tecnologia grant (PTDC/BIA-CEL/29765/2017). MVN and JC were supported by PhD fellowships from Fundação para a Ciência e Tecnologia (PD/BD/137442/2018 and PD/BD/136905/2018, respectively). We thank Paul Luzio (Cambridge Institute for Medical Research) for the critical reading of the manuscript. We also thank Silvia Benito-Martinez and Cédric Delevoye for sharing the ImageJ macro prior to publication and Jaime Mota (Faculdade de Ciências e Tecnologia, Universidade NOVA de Lisboa) for the kind gift of the Arl8b-GFP construct. We also thank the Microscopy, Cell Culture and Flow Cytometry facilities at NOVA Medical School Research and the Electron Microscopy Facility at Instituto Gulbenkian de Ciência.

AUTHOR CONTRIBUTIONS

Conceptualization: MVN, MJH, MCS, DCB; Formal Analysis: MVN, MJH, JC, CE; Funding Acquisition: MCS, DCB; Investigation: MVN, MJH, JC, CE; Methodology: MVN, MJH, JC, CE; Supervision: DCB, MCS; Writing - Original Draft Preparation: MVN, MJH, DCB; Writing - Review and Editing: MVN, MJH, JC, CE, MCS, DCB

SUPPLEMENTARY MATERIAL

Supplementary material is linked to the online version of the paper at www.jidonline.org, and at https://doi.org/10.1016/j.jid.2024.08.023.

REFERENCES

Agola JO, Hong L, Surviladze Z, Ursu O, Waller A, Strouse JJ, et al. A competitive nucleotide binding inhibitor: in vitro characterization of Rab7 GTPase inhibition. ACS Chem Biol 2012;7:1095–108.

Barral DC, Staiano L, Guimas Almeida C, Cutler DF, Eden ER, Futter CE, et al. Current methods to analyze lysosome morphology, positioning, motility and function. Traffic 2022;23:238–69.

Bento-Lopes L, Cabaço LC, Charneca J, Neto MV, Seabra MC, Barral DC. Melanin's journey from melanocytes to keratinocytes: uncovering the molecular mechanisms of melanin transfer and processing. Int J Mol Sci 2023;24:11289.

Borovanský J, Elleder M. Melanosome degradation: fact or fiction. Pigment Cell Res 2003;16:280–6.

Bright NA, Davis LJ, Luzio JP. Endolysosomes are the principal intracellular sites of acid hydrolase activity. Curr Biol 2016;26:2233–45.

Bright NA, Reaves BJ, Mullock BM, Luzio JP. Dense core lysosomes can fuse with late endosomes and are re-formed from the resultant hybrid organelles. J Cell Sci 1997;110:2027–40.

Burrinha T, Cunha C, Hall MJ, Lopes-da-Silva M, Seabra MC, Guimas Almeida C. Deacidification of endolysosomes by neuronal aging drives synapse loss. Traffic 2023;24:334–54.

Cantalupo G, Alifano P, Roberti V, Bruni CB, Bucci C. Rab-interacting lysosomal protein (RILP): the Rab7 effector required for transport to lysosomes. EMBO J 2001;20:683–93.

Cardoso MH, Hall MJ, Burgoyne T, Fale P, Storm T, Escrevente C, et al. Impaired lysosome reformation in chloroquine-treated retinal pigment epithelial cells. Invest Ophthalmol Vis Sci 2023;64:10.

Cichorek M, Wachulska M, Stasiewicz A, Tymińska A. Skin melanocytes: biology and development. Postepy Dermatol Alergol 2013;30:30–41.

Correia MS, Moreiras H, Pereira FJC, Neto MV, Festas TC, Tarafder AK, et al. Melanin transferred to keratinocytes resides in nondegradative endocytic compartments. J Invest Dermatol 2018;138:637–46.

Escrevente C, Falcão AS, Hall MJ, Lopes-da-Silva M, Antas P, Mesquita MM, et al. Formation of lipofuscin-like autofluorescent granules in the retinal pigment epithelium requires lysosome dysfunction. Invest Ophthalmol Vis Sci 2021;62:39.

Guardia CM, Farías GG, Jia R, Pu J, Bonifacino JS. BORC functions upstream of kinesins 1 and 3 to coordinate regional movement of lysosomes along different microtubule tracks. Cell Rep 2016;17:1950–61.

Hall MJ, Lopes-Ventura S, Neto MV, Charneca J, Zoio P, Seabra MC, et al. Reconstructed human pigmented skin/epidermis models achieve epidermal pigmentation through melanocore transfer. Pigment Cell Melanoma Res 2022;35:425–35.

Harada A, Takei Y, Kanai Y, Tanaka Y, Nonaka S, Hirokawa N. Golgi vesiculation and lysosome dispersion in cells lacking cytoplasmic dynein. J Cell Biol 1998;141:51–9.

Harrison RE, Bucci C, Vieira OV, Schroer TA, Grinstein S. Phagosomes fuse with late endosomes and/or lysosomes by extension of membrane protrusions along microtubules: role of Rab7 and RILP. Mol Cell Biol 2003;23:6494–506.

Hollenbeck PJ, Swanson JA. Radial extension of macrophage tubular lysosomes supported by kinesin. Nature 1990;346:864–6.

Hurbain I, Romao M, Sextius P, Bourreau E, Marchal C, Bernerd F, et al. Melanosome distribution in keratinocytes in different skin types: melanosome clusters are not degradative organelles. J Invest Dermatol 2018;138:647–56.

Jordens I, Fernandez-Borja M, Marsman M, Dusseljee S, Janssen L, Calafat J, et al. The Rab7 effector protein RILP controls lysosomal transport by inducing the recruitment of dynein-dynactin motors. Curr Biol 2001;11:1680–5.

Khatter D, Sindhwani A, Sharma M. Arf-like GTPase Arl8: moving from the periphery to the center of lysosomal biology. Cell Logist 2015;5:e1086501.

Marubashi S, Fukuda M. Rab7B/42 is functionally involved in protein degradation on melanosomes in keratinocytes. Cell Struct Funct 2020;45:45–55.

Matteoni R, Kreis TE. Translocation and clustering of endosomes and lysosomes depends on microtubules. J Cell Biol 1987;105:1253–65.

Minwalla L, Zhao Y, Le Poole IC, Wickett RR, Boissy RE. Keratinocytes play a role in regulating distribution patterns of recipient melanosomes in vitro. J Invest Dermatol 2001;117:341–7.

Moreiras H, Bento-Lopes L, Neto MV, Escrevente C, Cabaço LC, Hall MJ, et al. Melanocore uptake by keratinocytes occurs through phagocytosis and involves protease-activated receptor-2 internalization. Traffic 2022;23:331–45.

Moreiras H, Pereira FJC, Neto MV, Bento-Lopes L, Festas TC, Seabra MC, et al. The exocyst is required for melanin exocytosis from melanocytes and transfer to keratinocytes. Pigment Cell Melanoma Res 2020;33:366–71.

Moreiras H, Seabra MC, Barral DC. Melanin transfer in the epidermis: the pursuit of skin pigmentation control mechanisms. Int J Mol Sci 2021;22:4466.

Niwa S, Lipton DM, Morikawa M, Zhao C, Hirokawa N, Lu H, et al. Autoinhibition of a neuronal kinesin UNC-104/KIF1A regulates the size and density of synapses. Cell Rep 2016;16:2129–41.

Nixon RA. The aging lysosome: an essential catalyst for late-onset neurodegenerative diseases. Biochim Biophys Acta Proteins Proteom 2020;1868:140443.

Progida C, Cogli L, Piro F, De Luca A, Bakke O, Bucci C. Rab7b controls trafficking from endosomes to the TGN. J Cell Sci 2010;123:1480–91.

Pu J, Guardia CM, Keren-Kaplan T, Bonifacino JS. Mechanisms and functions of lysosome positioning. J Cell Sci 2016;129:4329–39.

Pu J, Schindler C, Jia R, Jarnik M, Backlund P, Bonifacino JS. BORC, a multisubunit complex that regulates lysosome positioning. Dev Cell 2015;33:176–88.

Rosa-Ferreira C, Munro S. Arl8 and SKIP act together to link lysosomes to kinesin-1. Dev Cell 2011;21:1171–8.

Tarafder AK, Bolasco G, Correia MS, Pereira FJC, Iannone L, Hume AN, et al. Rab11b mediates melanin transfer between donor melanocytes and acceptor keratinocytes via coupled exo/endocytosis. J Invest Dermatol 2014;134:1056–66.

van der Beek J, de Heus C, Liv N, Klumperman J. Quantitative correlative microscopy reveals the ultrastructural distribution of endogenous endosomal proteins. J Cell Biol 2022;221:e202106044.

Zoio P, Ventura S, Leite M, Oliva A. Pigmented full-thickness human skin model based on a fibroblast-derived matrix for long-term studies. Tissue Eng Part C Methods 2021;27:433–43.

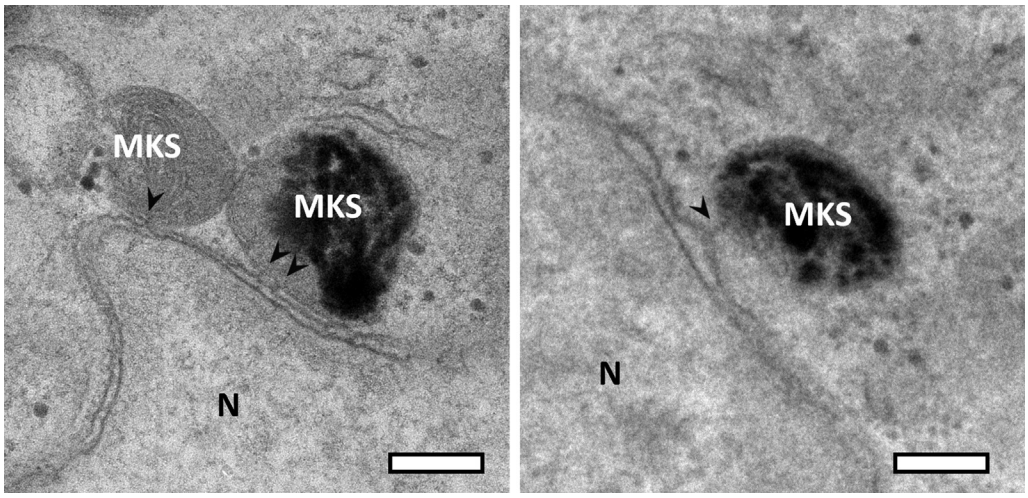

Supplementary Figure S1. MKS–nucleus tethers. MKSs in close apposition with the nucleus within keratinocytes of reconstructed human pigmented epidermis were observed by TEM. Areas of electron density that could represent protein tethers between the outer nuclear membrane and the MKS-limiting membrane are indicated by arrowheads. Bars = 200 nm. MKS, melanokerasome; N, nucleus; TEM, transmission electron microscopy.

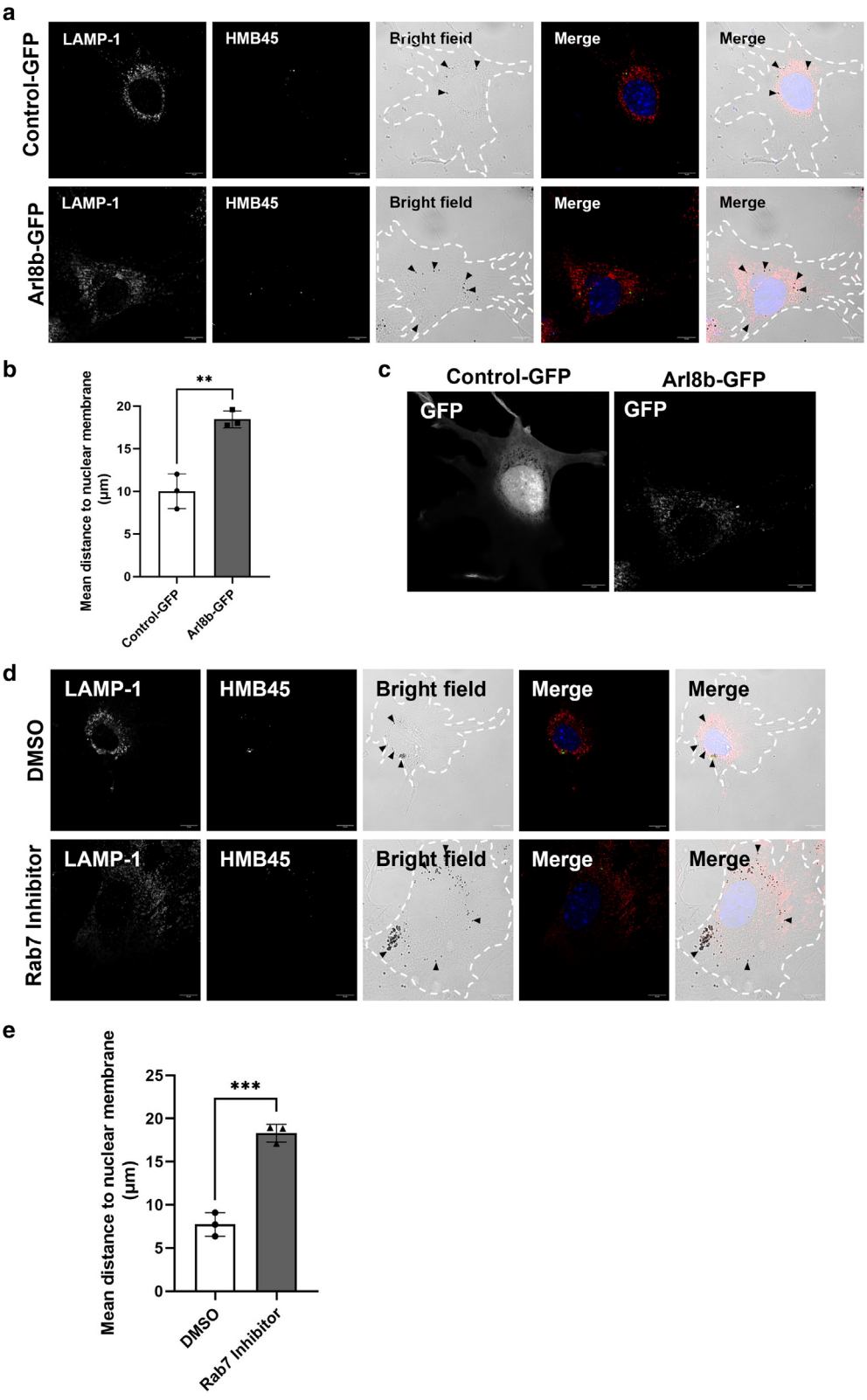

Supplementary Figure S2. Melanin juxtanuclear positioning is ablated upon Arl8 overexpression or Rab7 inhibition. **(a)** XB2 keratinocytes were transfected with nontargeting plasmid (control-GFP) or plasmid to overexpress Arl8b (Arl8b-GFP). Cells were then incubated with 0.1 g/l of melanocores for 4 hours, and melanin was chased for another 20 hours. After the chase, cells were fixed, and the distribution of melanocores inside keratinocytes was assessed by immunofluorescence. LAMP-1 (red) and HMB45 (green) antibodies were used to label late endosomes/lysosomes and PMEL17, respectively. Nuclei were visualized by DAPI staining (blue). Arrowheads indicate the melanocores inside keratinocytes. **(b)** Quantification of the mean distance of melanocores to the nuclear envelope. **(c)** Transfection efficiency was assessed by GFP expression. Bars = 10 μm. **(d)** XB2 keratinocytes were treated with either the vehicle drug (DMSO) or with 25 μm of Rab7 inhibitor. Simultaneously, cells were incubated with 0.1 g/l of melanocores, for 4 hours, and melanin was chased for 20 hours. Afterward, cells were fixed, and the distribution of melanocores inside keratinocytes was assessed by immunofluorescence. LAMP-1 (red) and HMB45 (green) antibodies were used to label late endosomes/lysosomes and PMEL17, respectively. Nuclei were visualized by DAPI staining (blue). Bars = 10 μm. Arrowheads indicate the melanocores inside keratinocytes. **(e)** Quantification of the mean distance of melanocores to the nuclear envelope. *P*-values (*t*-test) were considered statistically significant when <.01 (**) or <.001 (***) and ns when ≥.05. Plots shows mean ± SD of 3 independent experiments. ns, nonsignificant.

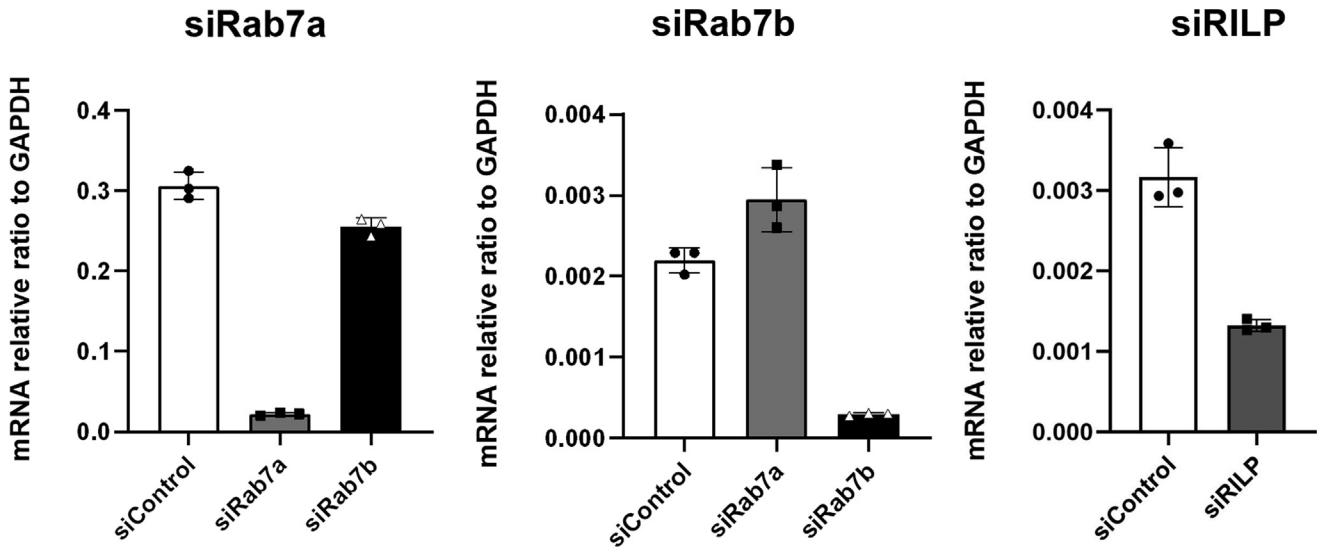

Supplementary Figure S3. Efficiency of siRNA silencing, assessed by qRT-PCR measurement of mRNA levels. XB2 keratinocytes were transfected with nontargeting siRNA (siControl) and siRab7a, siRab7b, or siRILP. The levels of silencing were measured by qRT-PCR, 72 hours after transfection. siControl, control-targeted small interfering RNA; siRab7a, Rab7a-targeted small interfering RNA; siRab7b, Rab7b-targeted small interfering RNA; siRILP, RILP-targeted small interfering RNA; siRNA, small interfering RNA.

Supplementary Table S1. siRNAs Used for Silencing

siRNA	Species	Reference
siControl	Mouse	D-001206-13
siRab7a	Mouse	M-040859-01
siRab7b	Mouse	M-053310-01
siRILP	Mouse	M-063866-01-0005

Abbreviations: siControl, nontargeting small interfering RNA; siRab7a, Rab7a-targeted small interfering RNA; siRab7b, Rab7b-targeted small interfering RNA; siRILP, RILP-targeted small interfering RNA; siRNA, small interfering RNA.

Supplementary Table S2. Plasmids Used for Overexpression

Overexpressed Protein	Plasmid Backbone	Source
GFP	pENTR-GFPC1	SicGen
Arl8b-GFP	pEGFP-N1	Jaime Mota

Supplementary Table S3. Primers Used for qRT-PCR

Primer	Species	Primer sequence (5′–3′)
Gapdh Forward	Mouse	AACTTTGGCATTGTGGAAGG
Gapdh Reverse		ACACATTGGGGGTAGGAACA
Rab7a Forward	Mouse	CCCCAACACTTTCAAAACCC
Rab7a Reverse		TGGCCCGGTCATTCTTGTCC
Rab7b Forward	Mouse	TCCAGAGTCCTTTGAAGCCC
Rab7b Reverse		AGCAGCATCTGCTCTTTGGC
Rilp Forward	Mouse	TGAGGATGAGGATGGCTCGT
Rilp Reverse		GCCTCAGTTTCACCCCGATA

Supplementary Table S4. List of Primary and Secondary Antibodies

Antibody	Host Species	Brand/Reference	Dilution
Anti-CD63	Mouse	MBL/R562	1:250
Anti-EEA-1	Mouse	BD Biosciences/ 610456	1:100
HMB45 (anti-PMEL)	Mouse	Dako/M0634	1:250
Alexa 647 anti-LAMP-1	Mouse	Santa Cruz/Sc19992	1:500
Alexa Fluor 488 anti-mouse	Goat	Invitrogen/A11001	1:500
Alexa Fluor 555 anti-mouse	Donkey	Invitrogen/A31570	1:500